

Experimental Study on the Seismic Behavior of Fault Gouge Induced by Fluid Injection

Li, W. Alghannam, M. and Juanes, R.

Massachusetts Institute of Technology, Cambridge, MA, USA

Copyright 2021 ARMA, American Rock Mechanics Association

This paper was prepared for presentation at the 55th US Rock Mechanics/Geomechanics Symposium held in Houston, Texas, USA, 20-23 June 2021. This paper was selected for presentation at the symposium by an ARMA Technical Program Committee based on a technical and critical review of the paper by a minimum of two technical reviewers. The material, as presented, does not necessarily reflect any position of ARMA, its officers, or members. Electronic reproduction, distribution, or storage of any part of this paper for commercial purposes without the written consent of ARMA is prohibited. Permission to reproduce in print is restricted to an abstract of not more than 200 words; illustrations may not be copied. The abstract must contain conspicuous acknowledgment of where and by whom the paper was presented.

ABSTRACT: Understanding the physical mechanisms controlling the fluid-injection-induced seismicity in the fault filled with gouge is crucial in the assessment and mitigation of induced seismicity, especially in the context of subsurface technologies like wastewater disposal, hydraulic fracturing, oil and gas production, geothermal energy extraction, and geologic storage of carbon dioxide.

Here, we study the seismic behavior of fault gouge induced by fluid injection experimentally with a novel ring shear apparatus. We designed this experimental setup to facilitate large shear strain, shear load stiffness control, normal stress and pore pressure control, and acoustic emission measurement. We use fine soda-lime spheres (~ 50 microns) as analog material for weakly-consolidated fault gouge. We load the gouge material to its critical state with the shear load stiffness controlled by a torsion spring. The fluid is injected with different pressurization rates to induce slip in the gouge. The results share many similarities with induced earthquakes, and shed light into how the pressurization rates affect the slip dynamics, providing the basis for novel constitutive modeling of fault friction.

1. INTRODUCTION

Fault gouge is crushed and ground-up rock produced by friction between the two sides when a fault moves (Scholz, 2019). Most natural faults are filled with fault gouge of various grain sizes depending on their stress and slip history. The frictional behavior of fault gouge controls the response of the fault formation to natural and industrial activities such as tectonic movements, groundwater level change, oil and gas production, water injection, and CO₂ storage (National Research Council, 2013). These responses could be aseismic or seismic, with various magnitudes of events. Therefore, it is important to understand the physical mechanisms controlling the fluid-injection-induced seismicity in the fault filled with gouge.

There are many experimental and theoretical studies on the seismic behavior of faults (Marone, 1998). The focus of the study has gradually shifted from studying the rate-and-state friction of the gouge material itself to studying the gouge with its mechanical and flow boundary conditions as a system (Marone et al., 1990; Linker and Dieterich, 1992; Segall and Rice, 1995; Ikari et al., 2009; Ougier-Simonin and Zhu, 2013; French et al., 2016; Leeman et al., 2016; Scuderi et al., 2017; Scuderi and Collettini, 2018, Cappa et al., 2019; Im et al., 2020; Wang et al., 2020a, 2020b). The experimental system has also evolved from simple two-axis mechanical control and measurements to the coupling with controlled shear stiffness, controlled pore pressure, and acoustic emission (AE) measurements. These studies provide valuable

insights into the seismic and aseismic behavior of fault gouge coupled with fluid.

Most of the studies mentioned above use either a triaxial system or a double shear system for the experimental research, which have a limited amount of slip distance. In addition, recent theoretical studies pointed out the importance of the pressurization rate on the seismic behavior of fault gouge, which few experimental studies covered.

Here we aim to overcome limitations in the amount of slip that can be achieved in triaxial shear and double shear systems. To do so, we designed a novel experimental setup configured as a ring shear apparatus to enable large shear strain, normal stress and pore pressure control, AE measurements and visual observations (Section 2). We conducted friction tests on dry and fluid-saturated gouge to characterize the frictional behavior of the gouge material. By adding a controlled shear stiffness (a torsion spring), we studied the stick-slip behavior of fault gouge with AE measurements (Section 3). We then used this system to study the effect of pressurization rates on the induced fault slip and seismicity (Section 4). Our experimental results are capable of quantitatively reproducing the main statistical laws describing seismicity. The results also provide qualitative experimental validation to the recent study on the pressurization rate dependence of fault slip: for the same amount of injected volume, lower injection rate builds up

lower pore pressure, and triggers less slip and less seismic events.

2. MATERIAL AND EXPERIMENTAL METHODS

2.1. Gouge Material

Soda-lime glass beads are used as an analog material to model the frictional behavior of fault gouge experimentally. As discussed by Dieterich and Kilgore (1994), soda-lime glass exhibits rate and state friction behavior similar to natural gouge materials, for example, granite gouge, but under lower normal stress than most rocks. Soda-lime glass spheres with a 50-micron median size were used in the experiments.

2.2. Experimental Setup

A computer-controlled ring shear apparatus was designed and built in the Juanes Research Group at MIT. Figure 1 shows the detailed design of the ring shear apparatus. A rotation stage is used to provide the driving force to the base of the ring shear. This rotation stage is controlled by a computer for accurate movement. The gouge material is filled in the groove of the base and sheared between the top ring and the groove base. The top ring is coupled with a torque-force sensor to measure normal and shear stresses. The rotation of the top ring is measured by a string pot with the string wound on a roller coupled with the torsion spring. The torsion spring provides controlled shear stiffness for the system. As discussed by Marone (1998), frictional stability should be studied as a system behavior, of which the stiffness of the system is a control variable. The other end of the torsion spring is connected to a load platen, which provides constant normal stress to the gouge material.

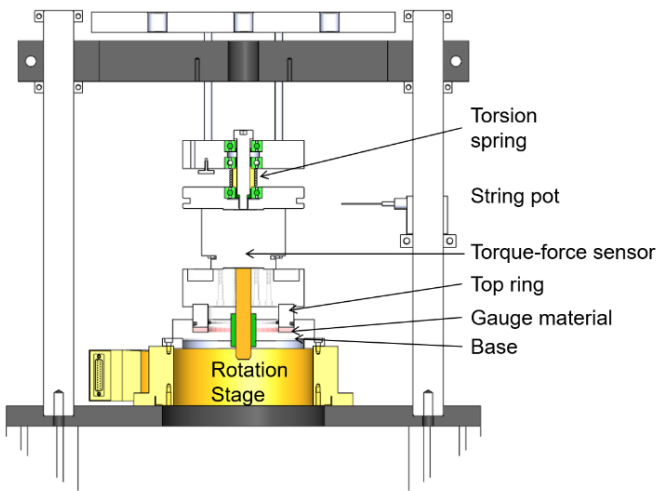


Fig. 1. Detailed design of the ring shear apparatus

This ring shear apparatus, comparing with the often-seen triaxial or double shear systems, has the advantage of having infinite slip distance. In addition, the apparatus is able to provide normal stress control, pore pressure

control, AE measurement, stiffness control, and visual observation.

The top ring has an inner radius (R_1) of 4.44 cm and an outer radius (R_2) of 6.35 cm. Thus, the area of the gouge under normal force (F_n) is:

$$A = \pi(R_2^2 - R_1^2) \quad (1)$$

The normal stress can be calculated as:

$$\sigma_n = \frac{F_n}{A} \quad (2)$$

The average radius (\bar{R}) to calculate slip distance is:

$$\bar{R} = \frac{\int_{R_1}^{R_2} r \cdot 2\pi r \cdot dr}{\int_{R_1}^{R_2} 2\pi r \cdot dr} = \frac{2}{3} \frac{R_2^3 - R_1^3}{R_2^2 - R_1^2} \quad (3)$$

The conversion from angular displacement to linear displacement is based on the average radius (\bar{R}). For example, the linear slip rate (v_L) can be calculated from the angular velocity (ω) as:

$$v_L = \omega \cdot \bar{R} \quad (4)$$

The measured torque (M) is an areal integration of the shear stress in the gouge. Assuming the shear stress (τ) is uniform in the gouge material, then the torque can be calculated as:

$$M = \int_{R_1}^{R_2} r \cdot 2\pi r \cdot \tau dr \quad (5)$$

Thus, the shear stress is calculated as:

$$\tau = \frac{M}{\frac{2\pi}{3}(R_2^3 - R_1^3)} \quad (6)$$

The results of the friction tests are presented using friction coefficient (μ) for stable slip and normalized shear stress (τ/σ_n) for stick-slip. The difference between these two parameters is that μ does not have an inertia term, but τ/σ_n does. However, they are both calculated by dividing the shear stress by the normal stress, as discussed by Im et al. (2020).

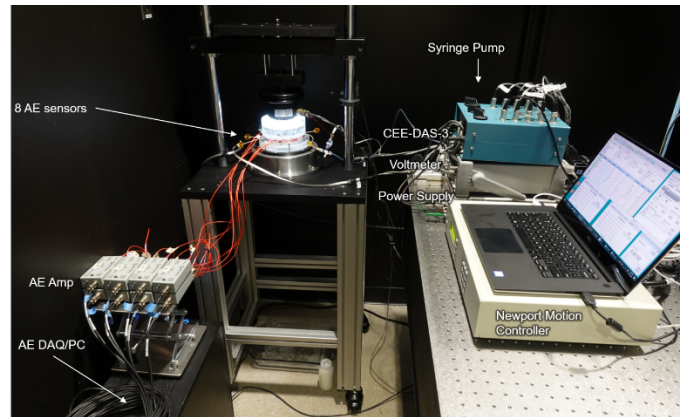


Fig. 2. Experimental setup for a ring shear test with pore pressure control and AE measurement

The experimental setup for a ring shear test with pore pressure control and AE measurement is shown in Fig. 2.

The computer on the right-side controls and monitors the rotation of the base, and the rate of injected volume. It monitors the normal stress, shear stress, top ring rotation, top ring axial displacement, inlet pressure and outlet pressure. AE is measured with eight AE sensors around the top ring (Fig. 3) and the data is recorded on a dedicated AE data acquisition system, as shown on the left side of Fig. 2.

The position of the eight AE sensors and the flow ports are shown in Fig. 3. The AE sensors are attached with hot glue counterclockwise around the top ring. There are in total six fluid ports, two of which are used as inlets connecting to the injection pump. A pressure sensor P1 is installed near one of the inlets to monitor the inlet pressure. Another two ports are used as outlets, with a pressure sensor P2 monitoring the outlet pressure.

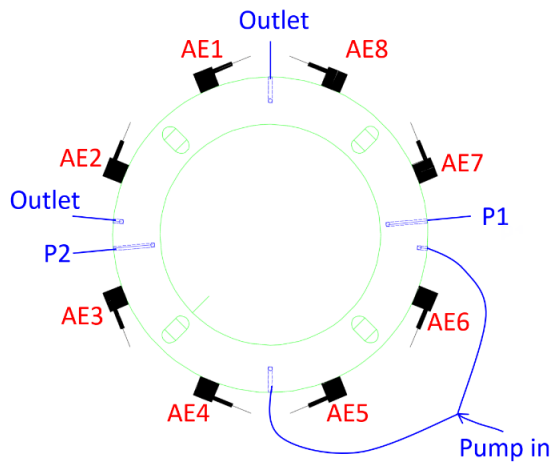


Fig. 3. Top view of the top ring with AE sensors (AE1-AE8), pore pressure sensors (P1 and P2), fluid- inlets and outlets.

3. FRICTION TESTS

3.1. Friction Tests with Dry and Fluid-Saturated Gouge

The gouge material was tested under dry- and wet (fluid-saturated) conditions in the ring shear apparatus to measure its friction coefficient. The test was done by removing the torsion spring and locking the shear stiffness control mechanism. With this significantly high stiffness of the system, the stable slip occurs during the tests. The measured friction coefficients under different normal stresses are summarized in Fig. 4.

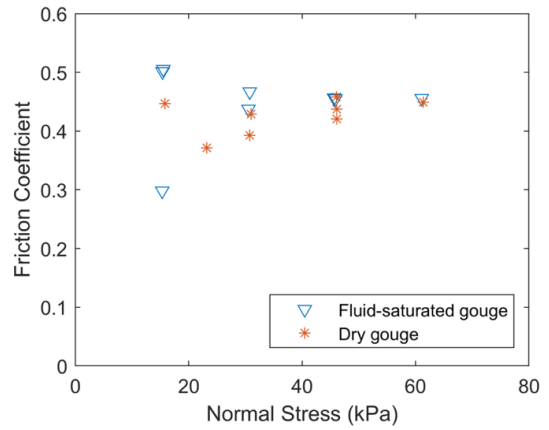


Fig. 4. Friction coefficient of the dry and fluid-saturated gouge.

The dynamic friction coefficient of the gouge is around 0.4, with some variations due to the normal stress. The fluid-saturated gouge has bigger variations in different tests because of the presence of water.

3.2. Friction Tests with Controlled Shear Stiffness

Friction tests are conducted to study the behavior of the fault gouge with controlled shear stiffness (torsion spring). Fig. 5 shows a friction test using the ring shear apparatus with AE measurements. In this test, the base rotates 540° at 1°/s rate. This corresponds to a linear shear loading rate of 1 mm/s. The torsion spring has a stiffness of 40 in-lb/90°, which is equivalent to 1 N/mm linear spring stiffness. The normal stress in the ring shear test is kept at 60 kPa for this test. The shear stress normalized by the normal stress is plotted with the blue line, while each AE event picked up by the AE sensors is plotted with red dots in Fig. 5.

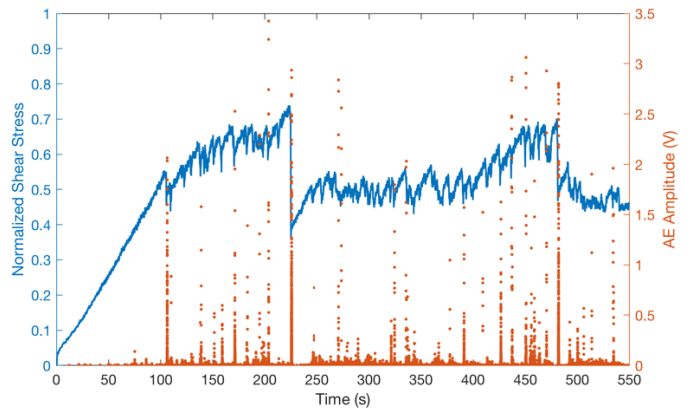


Fig. 5. Measured normalized shear stress and acoustic amplitude.

Because of the relatively low stiffness of the spring, the system shows stick-slip behavior. In the first 100 s, there is no slip occurring in the gouge material, so the base rotates and loads the torsion spring, as shown by the linearly increasing shear stress in Fig. 5. Then, the gouge material starts to slip, inducing the sudden drops in the shear stress and AE events. Larger slips induce greater

shear stress drops. The larger slips are also associated with more AE events with higher amplitudes.

4. FLUID INJECTION INDUCED FAULT SLIP

To study fluid injection induced fault slip, the ring shear tests are conducted by first loading the gouge to its critical state before slip occurs, then injecting fluid to trigger slips. These experimental processes mimic the case when faults are stressed by tectonic movement, then triggered by fluid injection. All three tests use a constant normal stress of 60 kPa. Each test injects with a constant flow rate (1.1 mL/min, 2.2 mL/min, 3.3 mL/min). 7.4 mL water is injected into the gouge, which is about 30% of the pore volume. A metering valve is used at the outlet to control the pressure dissipation at the outlet. The metering valve provides a constant hydraulic resistance to mimic the pore pressure dissipation in the gouge material.

Fig. 6 summarizes the results of the three tests. The gouge is loaded to its critical state, which corresponds to the shear stress of around 40 kPa. When the injection starts, the inlet and outlet pore pressures increase. Due to the high permeability of the gouge material, the inlet- and outlet pressures are very close. As the pore pressure increases, the slip is triggered and the shear stress drops. The stored elastic energy in the torsion spring then converts to frictional work and radiant seismic energy. The radiant energy is captured by the AE sensors, as shown by the AE events in Figure 6. After the injection, the pore pressure dissipates, following an exponential curve.

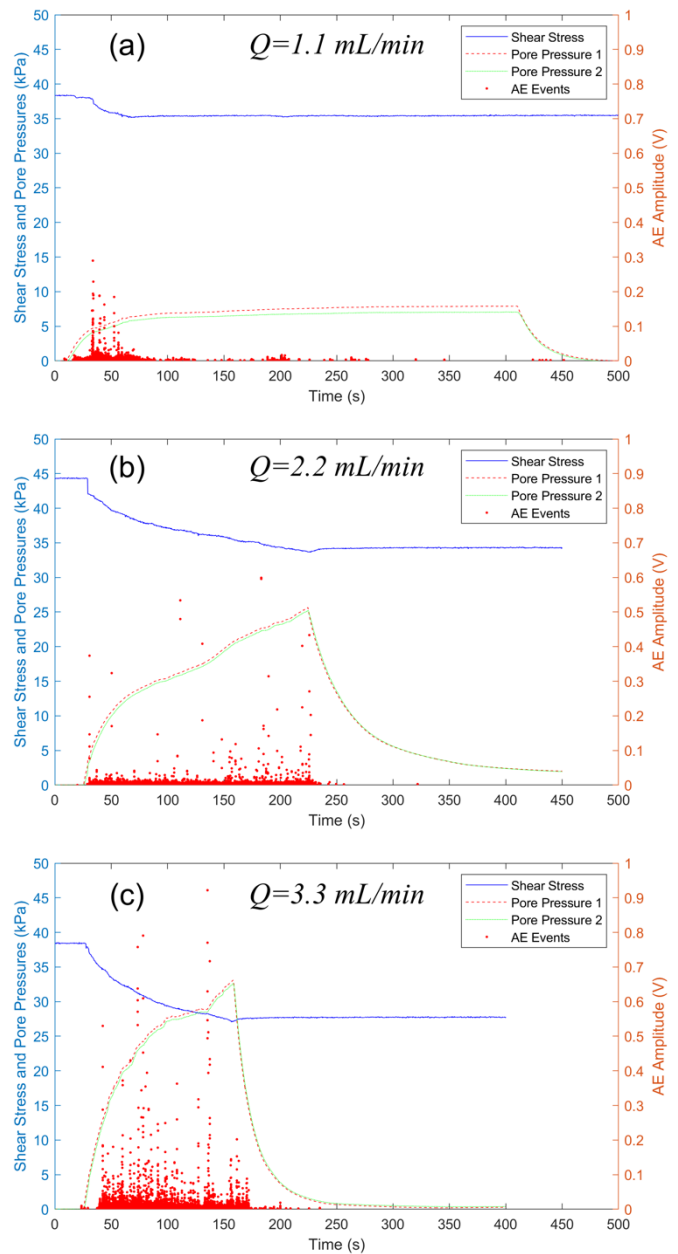


Fig. 6. Fluid injection induced fault slip.

The three tests show that for the same amount of fluid injection, a lower injection rate builds up lower pore pressure, and triggers less slip and fewer AE events. Most of the slips occur when the pressure is ramping up, showing a pressurization rate dependence. This is in-line with the theoretical predictions by Alghannam and Juanes (2020).

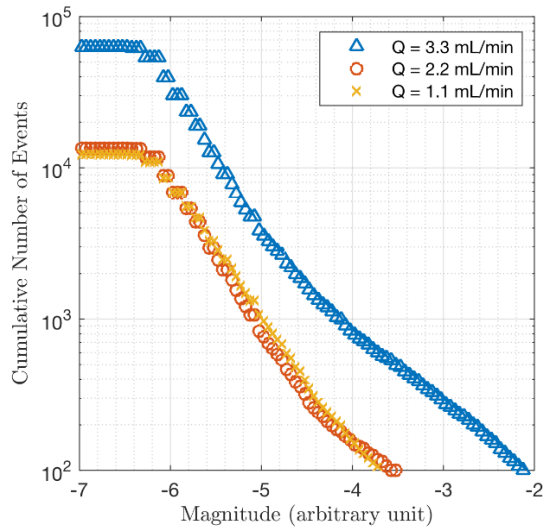


Fig. 7. Summary of the AE events.

The AE events for the three tests are summarized in Fig. 7. The distribution of the AE events is similar to the Gutenberg–Richter (GR) law. However, the curves have a more gradual slope near the high magnitude side, indicating that the seismicity induced by fluid injection proportionally has fewer high magnitude events comparing with the prediction of the GR law.

5. CONCLUSIONS

We study the seismic behavior of fault gouge induced by fluid injection experimentally with a novel ring shear apparatus. This ring shear apparatus facilitates large shear strain, shear load stiffness control, normal stress and pore pressure control, and AE measurement. We use fine soda-lime spheres (~ 50 microns) as analog material for weakly-consolidated fault gouge. We studied the friction behavior of dry and fluid-saturated gouge. By adding a controlled shear stiffness, we studied the stick-slip behavior of the fault gouge. These tests showed that the ring shear apparatus is capable of reproducing the friction behaviors found by using triaxial shear tests and double shear tests.

To study the seismic behavior of fault gouge induced by fluid injection, we first load the gouge material to its critical state with the shear load stiffness controlled by a torsion spring. The fluid is injected with different pressurization rates to induce slip in the gouge. The results share many similarities with induced earthquakes, and shed light into how the pressurization rates affect the slip dynamics: for the same amount of fluid injection, a lower injection rate builds up less pore pressure and triggers less slip and fewer AE events. Most of the slips occur when the pressure is ramping up, showing a pressurization rate dependence. The experimental results provide qualitative validation to the recent study on the

pressurization rate dependence of fault slip, and the basis for novel constitutive modeling of fault friction.

ACKNOWLEDGEMENT

This work was supported by the US Department of Energy (Grant No. DE-SC0018357).

REFERENCES

1. Alghannam, M., & R. Juanes. 2020. Understanding rate effects in injection-induced earthquakes. *Nature Communications*, 11(1), 1-6.
2. Cappa, F., M.M. Scuderi, C. Collettini, Y. Guglielmi and J.P. Avouac. 2019. Stabilization of fault slip by fluid injection in the laboratory and in situ. *Science Advances*, 5(3), p.eau4065.
3. Dieterich, J. H., and B. D. Kilgore. 1994. Direct observation of frictional contacts: New insights for state-dependent properties. *Pure and Applied Geophysics*, 143(1), 283-302.
4. French, M.E., W. Zhu and J. Banker. 2016. Fault slip controlled by stress path and fluid pressurization rate. *Geophysical Research Letters*, 43(9), 4330-4339.
5. Ikari, M.J., D.M. Saffer and C. Marone. 2009. Frictional and hydrologic properties of clay-rich fault gouge. *Journal of Geophysical Research: Solid Earth*, 114(B5).
6. Im, K., D. Saffer, C. Marone, and J. P. Avouac. 2020. Slip-rate-dependent friction as a universal mechanism for slow slip events. *Nature Geoscience*, 13(10), 705-710.
7. Leeman, J. R., D. M. Saffer, M. M. Scuderi, and C. Marone. 2016. Laboratory observations of slow earthquakes and the spectrum of tectonic fault slip modes. *Nature communications*, 7(1), 1-6.
8. Linker, M.F. and J.H. Dieterich. 1992. Effects of variable normal stress on rock friction: Observations and constitutive equations. *Journal of Geophysical Research: Solid Earth*, 97(B4), 4923-4940.
9. Marone, C., C.B. Raleigh and C.H. Scholz. 1990. Frictional behavior and constitutive modeling of simulated fault gouge. *Journal of Geophysical Research: Solid Earth*, 95(B5), 7007-7025.
10. Marone, C. 1998. Laboratory-derived friction laws and their application to seismic faulting. *Annual Review of Earth and Planetary Sciences*, 26(1), 643-696.
11. National Research Council. 2013. *Induced Seismicity Potential in Energy Technologies*. National Academies Press.
12. Ougier-Simonin, A. and W. Zhu. 2013. Effects of pore fluid pressure on slip behaviors: An experimental study. *Geophysical Research Letters*, 40(11), 2619-2624.

13. Sawai, M., A.R. Niemeijer, O. Plümper, T. Hirose and C.J. Spiers. 2016. Nucleation of frictional instability caused by fluid pressurization in subducted blueschist. *Geophysical Research Letters*, 43(6), 2543-2551.
14. Scholz, C. H. 2019. *The Mechanics of Earthquakes and Faulting*. Cambridge university press.
15. Scuderi, M. M., C. Collettini and C. Marone. 2017. Frictional stability and earthquake triggering during fluid pressure stimulation of an experimental fault. *Earth and Planetary Science Letters*, 477, 84-96.
16. Scuderi, M. M., and C. Collettini. 2018. Fluid Injection and the mechanics of frictional stability of shale-bearing faults. *Journal of Geophysical Research: Solid Earth*, 123(10), 8364-8384.
17. Segall, P., and J. R. Rice. 1995. Dilatancy, compaction, and slip instability of a fluid-infiltrated fault. *Journal of Geophysical Research: Solid Earth*, 100(B11), 22155-22171.
18. Wang, L., G. Kwiatek, E. Rybacki, A. Bonnelye, M. Bohnhoff, and G. Dresen. 2020a. Laboratory study on fluid-induced fault slip behavior: The role of fluid pressurization rate. *Geophysical Research Letters*, 47(6), e2019GL086627.
19. Wang, L., G. Kwiatek, E. Rybacki, A. Bonnelye, M. Bohnhoff, and G. Dresen. 2020b. Injection-induced seismic moment release and laboratory fault slip: Implications for fluid-induced seismicity. *Geophysical Research Letters*, 47(22), e2020GL089576.